undergo a pseudorotation before collapsing to product. Now, while there is of course no evidence that denies the possibility of enzyme-catalyzed pseudorotatory pathways, it has to be admitted that there is no enzymic reaction for which pseudorotation is a necessary (or even an attractive) step. Indeed, all known enzyme-catalyzed phospho group transfers can be accommodated mechanistically under the umbrella of simple in-line nucleophilic displacements. The only latitude for discussion concerns the relative extents of bond breaking and bond making at the transition state. In addition to these arguments, mechanism 2B involves a particularly unstable oxaphosphetane, and mechanism 2D (while enjoying, it must be said, excellent chemical precedent) clearly fails the test of mechanistic economy.

We are left, then, with the uncomplicated pathway involving a covalent phosphoenzyme intermediate, mechanism 2A. As pointed out in the introduction, other phosphomutases are known to involve the transient transfer of the phospho group to an enzyme nucleophile, and it seems most likely that the phosphoenolpyruvate mutase follows an analogous course. A search for the phosphoenzyme intermediate is underway.

Acknowledgment. We are grateful to Ted Widlanski and Eugene Mueller for helpful discussions, to Sonny Lee for assistance with crystal selection, and to the National Institutes of Health, the National Science Foundation, and Merck, Sharp and Dohme for support. S.F. is a Lister Institute Fellow. H.M.S. is a National Science Foundation Predoctoral Fellow.

Supplementary Material Available: Tables of bond distances and angles, selected torsion angles, hydrogen atom positions, anisotropic thermal parameters for non-hydrogen atoms, and a packing diagram for **1a** (6 pages); observed and calculated structure factors for **1a** (3 pages). Ordering information is given on any current masthead page.

Structural Analysis of a Low-Spin Cyanide Adduct of Iron(III) Transferrin by Angle-Selected ^{13}C ENDOR Spectroscopy

Penny A. Snetsinger,[†] N. Dennis Chasteen,*[,†] and Hans van Willigen[‡]

Contribution from the Department of Chemistry, University of New Hampshire, Durham, New Hampshire 03824-3598, and Department of Chemistry, University of Massachusetts at Boston, Boston, Massachusetts 02125. *Received November 20, 1989*

Abstract: A detailed analysis of powder-type ENDOR spectra of a ^{13}C-enriched cyanide adduct of transferrin was performed to obtain molecular and electronic structural information about the paramagnetic center. The low-spin, $S = {}^1/_2$, tricyano adduct is formed only in the C-terminal iron(III)-binding site of the protein and is characterized by a rhombic EPR spectrum having principle g factors of $g_{xx} = 2.34$, $g_{yy} = 2.15$, and $g_{zz} = 1.92$. A series of carbon-13 ENDOR spectra of a frozen solution sample at approximately 6 K were taken over the entire range of the EPR absorption. Only one set of ^{13}C ENDOR resonances was observed, which probably corresponds to only one or two of the CN groups, the other(s) being ENDOR silent. The ^{13}C nuclear hyperfine coupling is primarily isotropic with a small orientation-dependent dipolar component. The observed hyperfine coupling is a minimum along the g_{xx} axis and reaches a maximum along the g_{zz} axis, increasing nearly linearly between the two extremes. Simulations of the ENDOR line positions based on full-matrix calculations of the magnetic field selected subset of molecular orientations of the "powder" pattern indicate an isotropic coupling of $A_{iso} = -35.50$ MHz (assumed to be negative to be consistent with the couplings observed for other metal cyanide complexes) and dipolar couplings of $A_{aniso,xx} = 4.47$ MHz, $A_{aniso,yy} = -2.35$ MHz, and $A_{aniso,zz} = -2.12$ MHz. From an analysis of the orientation-dependent dipolar term it is concluded that the CN group giving rise to the ENDOR signals lies along the g_{xx} axis of the g tensor. By attributing the observed dipolar term solely to an electron–nuclear point dipole interaction from the unpaired electron centered on the iron, an Fe–^{13}C distance of 2.15 Å is calculated. A more extensive calculation in which the ground-state metal-based d_{xy} orbital of the electron is considered explicitly gives an Fe–^{13}C distance of 2.09 Å. The effect of the electron spin density in the carbon 2p orbital from the spin polarization mechanism on the calculated distance is discussed.

Introduction

The technique of electron nuclear double resonance (ENDOR) has proven to be a powerful tool in the study of electron–nuclear interactions in a number of iron proteins by affording resolution of ligand hyperfine interactions not observable with conventional electron paramagnetic resonance (EPR) spectroscopy.[1-3] The nuclear hyperfine tensors as measured by ENDOR spectroscopy can, in principle, be used to derive geometric and electronic structural information about the paramagnetic center. The most detailed spectroscopic information is obtained from single-crystal work. However, such an approach is often infeasible with biological systems such as metalloproteins in frozen solutions.

An especially promising development has been the use of orientation selection ENDOR by which single-crystal-type spectra can be obtained from a disordered powder or frozen solution. As first developed by Rist and Hyde, this technique concentrated on selected "pure orientations" contained within a powder EPR spectrum.[4] Recently, Hoffman[5,6] and Hurst et al.[7] have extended the theory of this technique to include ENDOR spectra taken over the entire range of EPR absorption. With the exception of the recent pioneering work by Hoffman and co-workers,[8,9] applications

[†] University of New Hampshire.
[‡] University of Massachusetts at Boston.

(1) Scholes, C. P. In *Multiple Electron Resonance Spectroscopy*; Dorio, M. M., Freed, J. H., Eds.; Plenum Press: New York, 1979; p 297.
(2) Mulks, C. F.; Scholes, C. P.; Dickinson, L. C.; Lapidot, A. *J. Am. Chem. Soc.* **1979**, *101*, 1645-1654.
(3) Sands, R. H. In *Multiple Electron Resonance Spectroscopy*; Dorio, M. M., Freed, J. H., Eds.; Plenum Press: New York, 1979.
(4) Rist, G. H.; Hyde, J. S. *J. Chem. Phys.* **1970**, *52*, 4633-4643.
(5) Hoffman, B. M.; Martinsen, J.; Venters, R. A. *J. Magn. Reson.* **1984**, *59*, 110-123.
(6) Gurbiel, R. J.; Hoffman, B. M. *J. Magn. Reson.* **1989**, *82*, 309-317.
(7) Hurst, G. C.; Henderson, T. A.; Kreilick, R. W. *J. Am. Chem. Soc.* **1985**, *107*, 7294-7299.
(8) Gurbiel, R. J.; Batie, C. J.; Sivaraja, M.; True, A. E.; Fee, J. A.; Hoffman, B. M.; Ballou, D. P. *Biochemistry* **1989**, *28*, 4861-4879.

0002-7863/90/1512-8155$02.50/0

of this technique to proteins have been limited and have not generally made full use of the angular selection information available in an anisotropic EPR spectrum. In the present work, we illustrate the use of such information by performing a detailed analysis of "off axis" powder-type ENDOR spectra of a cyanide adduct to obtain structural information about the metal center in a metalloprotein.

Although low-spin complexes of heme and hemoproteins are well-known,[10,11] low-spin cyanide adducts of non-heme iron(III) proteins are less well characterized. Recently, a number of iron–tyrosinate proteins and small-molecule analogues[12-14] that model the specific iron-binding site of these proteins have been shown to form low-spin adducts. Protocatechuate 3,4-dioxygenase[15,16] and human serum transferrin[17] both form low-spin cyanide adducts. Cyanide produces spectroscopically distinct low-spin complexes upon interaction with the high-spin metal center and isotopic substitution of both carbon and nitrogen is possible, making it ideal for magnetic resonance studies. Since the cyanide anion is often used as a probe of the exogenous ligand sites in metal protein complexes, it is of particular interest to explore the use of orientation-selected ENDOR to gain structural data about cyanide adducts in these complexes.

The transferrins are a class of non-heme, iron-binding proteins. The serum protein's main function is the transport of metabolic iron in the circulation of vertebrates.[18] All transferrins possess two separate iron-binding sites each contained in largely independent C and N lobes of the protein.[18,19] Both of these sites strongly bind iron in the +3 oxidation state and give rise to high-spin EPR signals at $g' = 4.3$ in the native protein. The addition of cyanide to diferric transferrin results in the formation of a low-spin adduct only at the C-terminal iron(III)-binding site, exhibiting a rhombic EPR absorption in the $g' = 2.0$ region of the spectrum.[17] The reaction for the formation of the cyanide adduct in this site is

$$Fe\text{–}Tf\text{–}CO_3^{z} + 3CN^- \rightarrow Fe\text{–}Tf\text{–}(CN)_3^{z-1} + CO_3^{2-}$$

where the (bi)carbonate anion is displaced from the first coordination sphere of the Fe(III) by cyanide. ENDOR has been used here to investigate the Fe(III)–CN interaction in the cyanide adduct of transferrin.

Experimental Section

The details of the preparation of the cyanide adduct of transferrin are given elsewhere.[17] The ^{13}C isotope was obtained as $Na^{13}CN$ from Icon Services in 91.5% purity. The protein concentration was 1 mM with a cyanide concentration of 0.5 M. Samples were run in 4-mm-o.d., 3-mm-i.d. quartz tubes.

ENDOR spectra were recorded with a Varian E-9 X-band spectrometer equipped with a home-built ENDOR accessory.[20,21] Temperatures of 6–8 K were obtained with an Oxford Instruments ESR9 helium cryostat. Typical spectra were recorded at 6 K, using 2-mW microwave power, approximately 200-W rf power, and frequency modulation of 10 KHz. A frequency counter was used to measure the EPR spectrometer frequency, and the free precessional frequency of protons from the matrix proton ENDOR signal was used to calibrate the magnetic field.

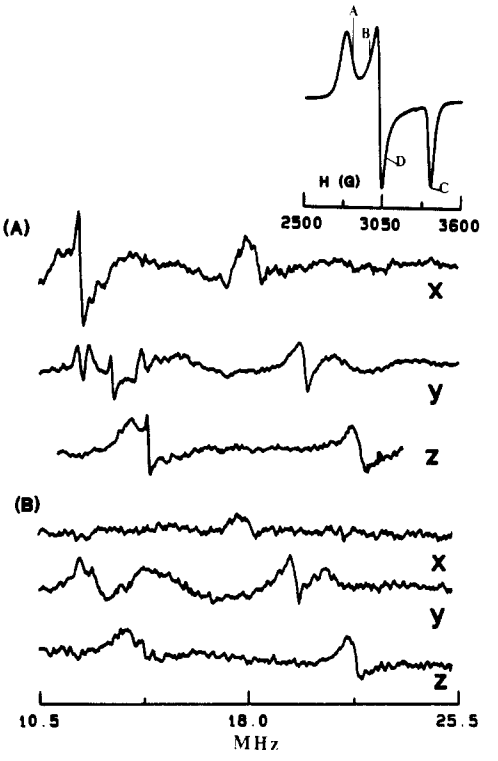

Figure 1. (A) ENDOR spectra of ^{13}CN–transferrin adduct at g_{xx} (H_0 = 2870 G), g_{yy} (H_0 = 3113 G), and g_{zz} (H_0 = 3458 G). (B) Same spectra as in (A) after subtraction of spectra ^{12}CN–transferrin from those of the ^{13}CN-enriched sample, thus removing all interactions due to nuclei other than ^{13}C. Experimental conditions: Temperature 8 K, center rf frequency 18 MHz, sweep width 15 MHz, microwave frequency 9.44 GHz, microwave power 2 mW, rf power 200 W, and frequency modulation 10 KHz. Inset: X-band EPR spectrum showing $g = 2$ region with ENDOR fields A, B, C, and D indicated. Experimental conditions: temperature 77 K, 0.58 mM protein, time constant 1 s, modulation amplitude 1.25 G, power 20 mW, frequency 9.36 GHz.

Results and Discussion

The ENDOR Spectrum. The addition of cyanide to transferrin results in a low-spin rhombic EPR spectrum at the C-terminal site with g factors $g_{xx} = 2.34$, $g_{yy} = 2.15$, and $g_{zz} = 1.92$[17] as shown in the inset of Figure 1. The ^{13}C hyperfine coupling is not resolved in the EPR spectrum, nor is any discernable broadening of the EPR line observed when [^{12}C]cyanide is replaced with [^{13}C]-cyanide.

^{13}C has a nuclear spin of $I = {}^1/_2$ and consequently gives rise to a two-line ENDOR pattern. In this case the electron–nuclear hyperfine interaction is greater than the nuclear Zeeman term so, to first order, the frequencies of the ENDOR lines are given by

$$\nu_{ENDOR} = |A_n|/2 \pm \nu_n \qquad (1)$$

where A_n ($A_{iso} + A_{aniso}$) is the sum of the ^{13}C isotropic coupling (A_{iso}) and anisotropic (A_{aniso}) hyperfine couplings and $\nu_n = g_n\beta_n H/h$ is the free precessional frequency of the ^{13}C nucleus in a magnetic field of strength H. Thus, one expects a pair of lines separated by $2\nu_n$ and centered at $|A_n|/2$.

Figure 1A shows the ENDOR spectrum of the transferrin–CN adduct at three different fields when prepared with isotopically enriched ^{13}CN. The lower frequency peak tends to be obscured by lines due to weakly coupled protons in the 12–14-MHz region. The proton interactions were removed by subtracting the spectrum of a transferrin–cyanide adduct prepared with ^{12}CN (Figure 1B). Since ^{12}C has a nuclear spin of zero, it does not contribute to the ENDOR spectrum; however, the interactions of all other nuclei, including protons, will be identical. This subtraction effectively

(9) True, A. E.; Nelson, M. J.; Venters, R. A.; Orme-Johnson, W. H.; Hoffman, B. M. *J. Am. Chem. Soc.* **1988**, *110*, 1943–1950.
(10) Scholes, C. P.; Van Camp, H. L. *Biochim. Biophys. Acta* **1976**, *434*, 290–296.
(11) LoBrutto, R. L.; Wei, Y. H.; Mascarenhas, R.; Scholes, C. P.; King, T. E. *J. Biol. Chem.* **1983**, *258*, 7437–7448.
(12) Spartalian, K.; Carrano, C. J. *Inorg. Chem.* **1989**, *28*, 19–24.
(13) Carrano, C. J.; Carrano, M. W.; Sharma, K.; Backes, G.; Sanders-Loehr, J. *Inorg. Chem.* **1990**, *29*, 1865–1870.
(14) McDevitt, M. R.; Addison, A. W.; Sinn, E.; Thompson, L. K., submitted for publication.
(15) Wittaker, J. W.; Lipscomb, J. D. *J. Biol. Chem.* **1984**, *259*, 4487–4495.
(16) Orville, A. M.; Lipscomb, J. D. *J. Biol. Chem.* **1989**, *264*, 8791–8801.
(17) Swope, S. K.; Chasteen, N. D.; Weber, K. E.; Harris, D. C. *J. Am. Chem. Soc.* **1988**, *110*, 3835–3840.
(18) Chasteen, N. D. In *Iron Binding Proteins without Cofactors or Sulfur Clusters*; Advances in Inorganic Biochemistry Vol. 5; Theil, E. C., Eichorn, G. L., Marzilli, L. G., Eds.; Elsevier: New York, 1983; pp 201–233.
(19) Bailey, S.; Evans, R. W.; Garratt, R. C.; Gorinsky, B.; Hasnain, S.; Horsburgh, C.; Jhoti, H.; Lindley, P. F.; Mydin, A.; Sarra, R.; Watson, J. L. *Biochemistry* **1988**, *27*, 5804–5812.
(20) van Willigen, H. *J. Magn. Reson.* **1980**, *39*, 37–46.
(21) Mulks, C. F.; van Willigen, H. *J. Phys. Chem.* **1981**, *85*, 1220–1224.

removes all peaks due to nuclei other than ^{13}C. As expected, a two-line spectrum is observed with a splitting twice the appropriate Zeeman frequency for ^{13}C.

Angle-Selective ENDOR. Setting the external field $\vec{H}$ within the EPR envelope of a polycrystalline sample to obtain ENDOR spectra corresponding to particular orientations has been discussed extensively.[4,5,22] The samples employed in this study are frozen solutions and thus contain a random distribution of all protein orientations. Since rf irradiation at any field within the EPR spectrum allows one to select a distinct group of limited molecular orientations, the anisotropy in the EPR spectrum can be exploited to obtain a series of ENDOR spectra, each representing a different subset of molecular orientations.

To locate the CN position within the coordinate system of the **g** tensor, ENDOR spectra were taken every 50 G in the range 2850–3500 G (g_{xx} to g_{zz}). Since the proton ENDOR lines overlap with the lower frequency ^{13}C line at all fields, only the position of the higher frequency peak was accurately measured and fitted in subsequent full-matrix calculations.

The position of the higher frequency ^{13}C peak increases almost linearly with increasing magnetic field. Some of the increase is due to the increase in the free precessional frequency of the nucleus with field and the remainder is due to the anisotropic component of the ^{13}C nuclear hyperfine interaction. The small change in $|A_n|$ from a minimum of 30.53 MHz at g_{xx} to a maximum of 37.17 MHz at g_{zz} indicates that the coupling is primarily isotropic with a small anisotropic component (A_{aniso}), which varies according to the molecular orientations selected by the field position in the EPR spectrum. For strictly isotropic coupling, there would be no change in the value of $|A_n|$ with field.

Isotropic Coupling. The considerable isotropic component arises from s-orbital electron spin density on the carbon. Direct coordination of ^{13}C to the Fe(III) site is indicated by the magnitude of the coupling. Couplings with similar magnitudes (28.64 and 27.33 MHz) have been reported in studies of ^{13}C–heme complexes.[23] Analysis of the g factors of the transferrin adduct indicates that the unpaired electron is in an orbital that is mainly d_{xy} in character in the coordinate system of the **g** tensor.[17] Since the carbon s orbital has the wrong symmetry to bond directly to the d_{xy} orbital, the isotropic coupling cannot be due to the traditional Fermi contact term. A large contact interaction of negative sign (approximately −30 MHz), which is observed with metal cyanide complexes, has been attributed to an exchange polarization mechanism between an unpaired electron in the metal d orbital and paired electrons in a cyanide σ orbital.[24] NMR work has confirmed the sign of this coupling for aqueous $K_3Fe(CN)_6$ and $K_4Fe(CN)_6$.[25] The magnitude of the isotropic hyperfine coupling for the cyanide adduct of transferrin ($|A_{iso}|$ = 35.5 MHz) is in substantial agreement with hyperfine couplings for other transition-metal cyanide complexes. These couplings are largely isotropic and of negative sign.[24-26] Therefore, we assume that the sign of the isotropic coupling in transferrin is likewise negative.

The sign of the dipolar hyperfine coupling for different magnetic fields is dependent on the location of the CN group in the axis system of the **g** tensor. The minimum apparent coupling $|A_n|$ is along g_{xx}, and the maximum along g_{zz}. This is consistent with the CN group being located on the x axis. For the magnetic field aligned along g_{xx}, a maximum positive dipolar coupling is expected which when added to the negative isotropic coupling results in a total coupling of less magnitude than the isotropic coupling alone. Along g_{zz} the maximum negative dipolar coupling adds to the negative isotropic coupling, resulting in a maximum magnitude of the total coupling. Full-matrix calculations show that moving the CN group only a few degrees off the x axis changes the dipolar coupling sufficiently that the variation in the ^{13}C hyperfine coupling across the EPR spectrum no longer matches that of the data (vide infra). Thus, the location of the ^{13}C on the x axis or within ±5° of it is firmly established. As is illustrated below, the small but readily measured dipolar component contains useful information.

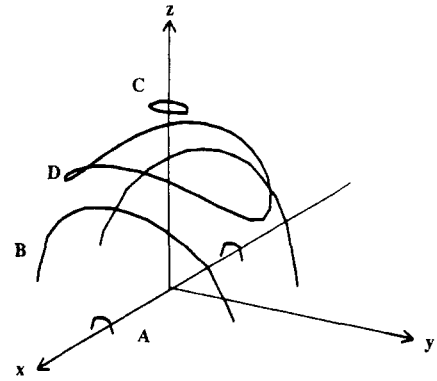

Figure 2. Unit sphere (only top half is shown) with curves (or pairs of curves for the case of A and B) of constant g. Each line represents all sets of θ and ϕ that satisfy eq 3 for a particular g value. Field is 2925 G for A, 3075 G for B, 3500 G for C, and 3225 G for D as indicated in Figure 1 inset. Microwave frequency is 9.44 GHz.

Simulations. Simulations of the ENDOR spectra[27] were based on the approach by Hurst et al.[7] The general method of simulation is to determine the molecular orientations that will contribute to the ENDOR at a given field value H in the EPR. The EPR spectrum is first simulated to determine allowed transitions at that field. Thus, a distinct set of molecular orientations giving rise to transitions within the EPR at a given field value is obtained. In effect, the external field "selects" certain molecular orientations according to g anisotropy in the spectrum. Because the spectrum of transferrin is dominated by g anisotropy, i.e., the electron–ligand nuclei couplings are small, and the metal nuclear spin is zero, the appropriate spin Hamiltonian for the EPR experiment is given by

$$\hat{\mathcal{H}} = \beta_e \vec{H} \cdot \overleftrightarrow{g} \cdot \hat{\mathbf{S}} \tag{2}$$

where the required resonance condition is

$$H_r = h\nu / g(\theta, \phi)\beta_e \tag{3}$$

where

$$g(\theta, \phi) = [(g_{xx} \sin\theta \cos\phi)^2 + (g_{yy} \sin\theta \sin\phi)^2 + (g_{zz} \cos\theta)^2]^{1/2}$$

Thus a specific magnetic field, $\vec{H}$, within the EPR spectrum, will give a set of θs and ϕs for which eq 3 is satisfied.[28] The set of θs and ϕs represents all orientations giving rise to the same g value as illustrated in Figure 2. However, each θ–ϕ combination will give different ENDOR resonances since the dipolar interactions with ligand nuclei change with each θ–ϕ combination. Thus, the ENDOR spectrum reflects the angular dependence of hyperfine energies of the ligand nuclei. Figure 3 shows the results of calculations illustrating this effect on the ENDOR spectrum. Here the ^{13}C nucleus is placed on the molecular g_{xx} axis. At the edges of the EPR spectrum, near g_{xx} and g_{zz} (peaks A and C in Figure 3), there is only a narrow range of ENDOR frequencies. At intermediate field values between g_{xx} and g_{zz} (Figure 3, peak

(22) Hutchinson, C. A.; McKay, D. B. *J. Chem. Phys.* **1977**, *66*, 3311–3330.
(23) Mulks, C. F.; Scholes, C. P.; Dickinson, L. C.; Lapidot, A. *J. Am. Chem. Soc.* **1979**, *101*, 1645–1654.
(24) Kuska, H. A.; Rogers, M. T. *J. Chem. Phys.* **1964**, *41*, 3802–3805.
(25) Lowenstein, A.; Shporer, M.; Navon, G. *J. Am. Chem. Soc.* **1963**, *85*, 2855–2856.
(26) Davis, D. G.; Kurland, R. G. *J. Chem. Phys.* **1967**, *46*, 388–390.
(27) The program ANGSEL, which calculates the orientations contributing to the ENDOR spectrum and the ENDOR frequencies, was a modified version of the program described in ref 7 and was obtained from Dr. J. B. Cornelius of the Biotechnology Resource in Pulsed EPR Spectroscopy at the Albert Einstein College of Medicine.
(28) A computer search was used to determine values for θ and ϕ that satisfy eq 3. However, an analytic function that relates θ and ϕ at a given g value has been reported.[5]

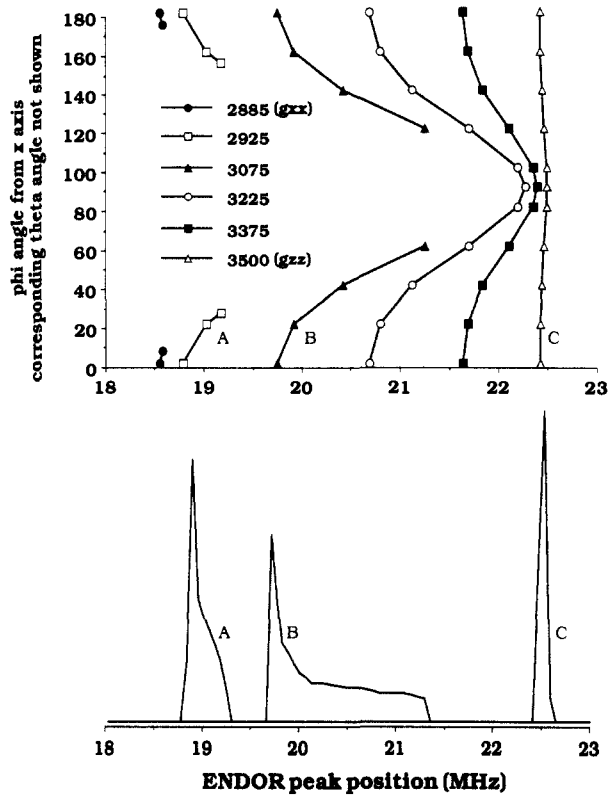

Figure 3. Simulations showing the dependence of the ENDOR absorption frequency (in MHz) for magnetic fields ranging from approximately g_{xx} to g_{zz} in the EPR spectrum. ϕ is the angle described in eq 3 for orientations from 0 to 180°. Only the higher frequency peak of the ENDOR pair of lines is shown. Simulation assumes ^{13}C nucleus along g_{xx} axis with a point dipole interaction. A, B, and C correspond to the field positions indicated in Figure 1 inset and Figure 2.

B) a wider range of frequencies becomes possible, giving rise to partial "powder" patterns in the ENDOR.

ENDOR spectra observed along the two edges of the EPR absorption spectrum, (i.e., along g_{xx} and g_{zz}) give true "single-crystal"-like spectra, representing essentially pure orientations (Figure 2).[4,29] Since, between these two extremes a variety of orientations contributes to the ENDOR spectrum, two turning points or edges in the ENDOR "powder" pattern are observed and broadening of the observed ENDOR peaks is expected. The range of ^{13}C frequencies contributing to the ENDOR peak at a given field is determined by the anisotropy in the **g** tensor. In the case of transferrin, the largest difference between the high and low edges of the simulated absorption peak is 1.7 MHz. Figure 4 shows that including a line width similar to that observed experimentally results in a derivative crossing point corresponding closely to the most intense absorption side of the simulated ENDOR peak. Consequently, we have chosen to match the higher intensity turning point of the simulated peak with the experimental peak location. Since our interest was in the position of the ^{13}C peak, no attempt was made to match either the ENDOR line shape or its intensity. Figure 5 shows the results of the simulated ENDOR peak position as a function of EPR field compared with the experimental values. The positions of both the high and low edges of the ENDOR peak are shown. Excellent agreement between the low-frequency (higher intensity) edge and the experimental data is obtained.

Analysis of Anisotropic Coupling. The anisotropic electron–nuclear hyperfine coupling tensor arrived at from our simulations has elements

$$A_{\text{aniso},xx} = 4.47 \text{ MHz} \qquad A_{\text{aniso},yy} = -2.35 \text{ MHz}$$
$$A_{\text{aniso},zz} = -2.12 \text{ MHz} \qquad (4)$$

(29) Schweiger, A.; Wolf, R.; Gunthard, Hs. H.; Ammeter, J. H.; Deiss, E. *Chem. Phys. Lett.* **1980**, *71*, 117–122.

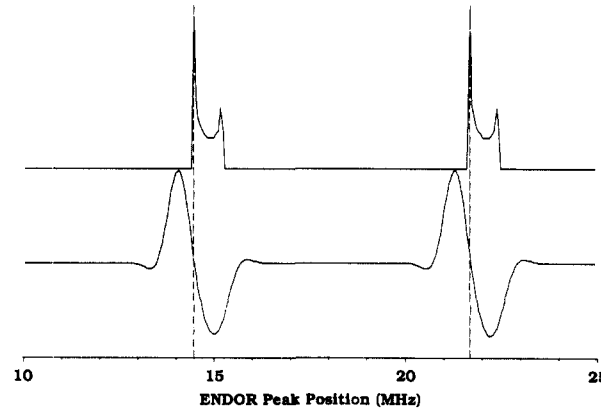

Figure 4. Simulation of ENDOR peaks at $g = 2.17$ ($H_0 = 3075$ G). Top shows the simulated ENDOR "powder" pattern obtained from the subset of molecular orientations corresponding to $g = 2.17$. Bottom is the derivative of this same simulation after including a line width of 0.94 MHz, similar to those observed experimentally. The derivative crossing point corresponds to the high-intensity side of the simulated peak.

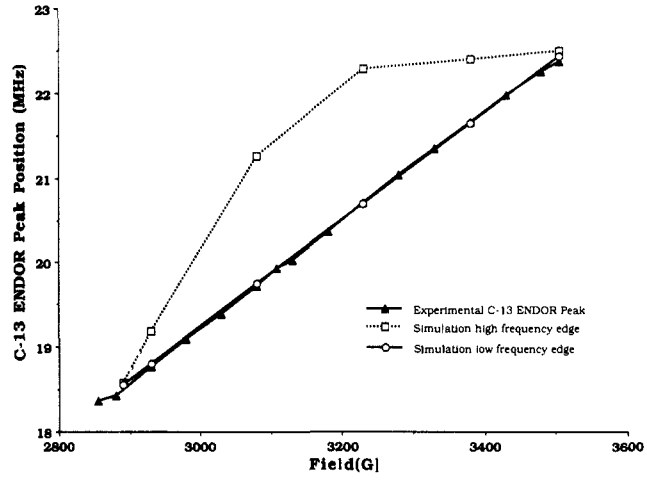

Figure 5. Comparison of ENDOR simulation (higher frequency peak of the ENDOR pair only) with experimental results. Both the high- and low-frequency edges of the simulated peak are shown. The calculation assumes the ^{13}C nucleus is located on the g_{xx} axis at a distance of 2.15 Å with an isotropic coupling of −35.50 MHz and a point dipole interaction for the anisotropic coupling. Errors in experimental peak position are nominally ±0.1 MHz.

The Fe–^{13}C distance can be estimated from the anisotropic coupling A_{aniso} by assuming that this coupling is solely due to the through-space dipolar interaction, A_d. The tensor elements of this dipole–dipole interaction are given in Chart I, where r is the distance between the ^{13}C and the iron, g_n is the nuclear g factor for ^{13}C, β_e and β_n are the Bohr and nuclear magnetons, respectively, and θ_N and ϕ_N are the polar angles of the nucleus relative to the principal axis system for the **g** tensor.

The point dipole approximation is generally considered valid for distances on the order of 2.5 Å or greater with weak contact interaction.[30] Although that is obviously not the case here, a simple dipole calculation nevertheless gives an Fe–^{13}C distance of 2.15 Å, a result in reasonable agreement with the bond distances of 1.8–1.9 Å typically found for metal cyanide complexes.[31–33]

To obtain a better estimate of the iron–carbon distance, the dipole interaction was calculated by explicitly using the ground-state d_{xy} orbital for the unpaired electron. The details of the

(30) Schweiger, A. *Struct. Bonding (Berlin)*; Springer Verlag: Berlin, 1982; Vol. 51, p 50.
(31) Curry, N. A.; Runciman, W. A. *Acta Crystallogr.* **1959**, *12*, 674–678.
(32) Maer, K.; Beasley, M. L.; Collins, R. L.; Milligan, W. O. *J. Am. Chem. Soc.* **1968**, *90*, 3201–3208.
(33) Gupta, M. P.; Milledge, H. J.; McCarthy, A. E. *Acta Crystallogr.* **1974**, *B30*, 656–661.

Chart I

$$\overleftrightarrow{A}_d = \frac{-\beta_e\beta_n g_n}{hr^3}\begin{pmatrix} g_{xx}((3\cos\phi_N\sin\theta_N)^2-1) & 3g_{xx}\cos\phi_N\sin^2\theta_N\sin\phi_N & 3g_{xx}\cos\phi_N\sin\phi_N\cos\theta_N \\ 3g_{yy}\cos\phi_N\sin^2\theta_N\sin\phi_N & g_{yy}((3\sin\phi_N\sin\theta_N)^2-1) & 3g_{yy}\sin\phi_N\sin\theta_N\cos\theta_N \\ 3g_{zz}\cos\phi_N\sin\phi_N\cos\theta_N & 3g_{zz}\sin\phi_N\sin\theta_N\cos\theta_N & g_{zz}((3\cos\theta_N)^2-1) \end{pmatrix} \quad (5)$$

lengthy calculation are given in the Appendix. The use of the eqs 1A–3A instead of the point dipole approximation (eq 5) changes the distance only slightly from 2.15 to 2.09 Å. Thus, it is evident that the point dipole approximation is reasonably good for estimating distances even at bond lengths approaching 2 Å. This result appears to be due largely to the contracted nature of the transition-metal-based d orbital.

In addition to the dipolar interaction discussed above, there are other contributions to the observed anisotropic coupling due to the electron–nuclear interaction from the unpaired electron spin density in the ^{13}C p orbitals. There is a contribution to $f_\sigma A_p$, which arises from the σ bond of the carbon p_x orbital, and there are two π-type interactions, $f_{\pi 1}A_p$ and $f_{\pi 2}A_p$, due to spin density from back-bonding involving the iron d_{xz} and d_{xy} orbitals and the cyanide p_z and p_y orbitals, respectively. Thus, the total anisotropic coupling (A_{aniso}) is given by

$$A_{aniso,xx} = (2A_d + 2f_\sigma A_p - f_{\pi 1}A_p - f_{\pi 2}A_p)g_{xx}/g_e \quad (6)$$

$$A_{aniso,yy} = (-A_d - f_\sigma A_p + 2f_{\pi 1}A_p - f_{\pi 2}A_p)g_{yy}/g_e$$

$$A_{aniso,zz} = (-A_d - f_\sigma A_p - f_{\pi 1}A_p + 2f_{\pi 2}A_p)g_{zz}/g_e$$

where f_σ and f_π are the spin densities in the carbon p orbitals giving rise to σ bonding and π bonding, respectively.

A value for f_σ can be estimated from the isotropic coupling A_{iso}. The isotropic coupling of −35.50 MHz corresponds to a spin density of 1.14% in the carbon s orbital (unit spin density giving a coupling of 3110 MHz for ^{13}C;[34] 35.5/3110 × 100 = 1.14%). A similar spin density is anticipated for the σ-bonding carbon p orbital since the σ bond between carbon and iron to the first approximation involves a carbon sp hybrid orbital. Thus, the contribution to the anisotropic coupling for the case of an sp hybrid would be 1.04 MHz, or 1.14% of 90.8 MHz (unit spin density in a carbon p orbital gives an anisotropic coupling A_p of 90.8 MHz for ^{13}C[34]). As described for the isotropic coupling, this spin density arises from a spin-polarization mechanism, and consequently, f_σ (= −0.0114) should be negative. If the $f_{\pi 1}$ and $f_{\pi 2}$ terms in eq 6 are neglected, the anisotropic components due to the dipolar interaction from the metal alone would then be

$$A_{d,xx} = 6.90 \text{ MHz} \qquad A_{d,yy} = -3.47 \text{ MHz}$$
$$A_{d,zz} = -3.12 \text{ MHz} \quad (7)$$

These couplings lead to a decrease in the calculated distance between the iron and the ^{13}C nucleus from 2.15 to 1.86 Å,[35] using the point dipole approximation.

The 1.86-Å bond length is very close to those obtained from X-ray studies of metal cyanide complexes. However, we have neglected in our calculations the π-bonding terms of eq 6 (which may be appreciable[36]) as well as delocalization of the unpaired electron onto other ligands in the metal site. Thus, the good agreement with X-ray results may be simply due to fortuitous cancellation of various contributions to the anisotropic coupling.

Conclusion. The structure originally proposed for the cyanide adduct of transferrin includes three cyanides coordinated to the iron center in the C-terminal domain.[17] However, only one pair of ^{13}C lines was observed in the current ENDOR study. There are a number of situations that could give rise to the single set of ^{13}C peaks:

(1) While three cyanides are involved in the conversion of the iron(III) to low spin, only one cyanide may actually be bound to the metal center. The possibility that some of the CN^- groups bind to cationic sites on the protein, causing a conformational change leading to a low-spin complex, was suggested in the previous study.[17] The binding of simple inorganic anions such as chloride and perchlorate to transferrin causing a change in the spectral, kinetic, and thermodynamic properties of the iron, particularly in the C-terminal site, is well-known.[37–39]

(2) The set of peaks may represent two coordinating cyanide groups trans to one another with the same ^{13}C couplings. Trans cyano complexes are known.[40] From the structure of the metal site in transferrin,[19,41,42] we would expect trans coordination of two cyanides to result in the rearrangement of protein ligands.

(3) There may be three cyanides bound to the iron with only one or two of them being ENDOR visible. For example, cyanide(s) located on the z axis may have a ^{13}C coupling with the unpaired electron in the d_{xy} orbital that is too small to be observed.

Although the ENDOR study of the cyanide adduct of transferrin does not provide additional information about the number of cyanides bonded to the metal center, it does definitively locate at least one of the three cyanide groups of the adduct. Analysis of the orientation dependence of the dipole interaction places this CN^- along the g_{xx} axis at a distance consistent with the X-ray bond lengths for other metal cyanide complexes. The detailed analysis reported in the present paper illustrates the application of ENDOR of "powdered" samples to studies of cyanide adducts of metalloproteins. This technique should be applicable to studies of the structure and bonding of small mixed-ligand Fe(III) cyano complexes in frozen solution as well.

Acknowledgment. This work was supported by National Institutes of Health Grant GM-20194. We thank Dr. Brian M. Hoffman for his suggestions regarding the spin polarization contribution to the dipole calculation.

Appendix

To obtain a better estimate of the ^{13}C–iron distance, the dipolar interaction of a point nucleus located on the x axis with an electron in a metal-based d_{xy} orbital is calculated. This problem can be treated in a manner similar to the well-known case of an α-proton with a carbon p orbital,[43,44] although the integrals obtained in the present work are more complex. In order to simplify the calculation, the case of a d_{yz} orbital with the nucleus along the z axis is considered. The results for the x axis–d_{xy} orbital case follow simply from the z axis–d_{yz} case.

(34) Wertz, J. E.; Bolton, J. R. *Electron Spin Resonance*; New York: McGraw Hill: New York, 1972; Table C.

(35) The limit that the anisotropic component of approximately 2.2 MHz is due completely to electron spin density in a carbon 2p orbital (where unit spin density gives a coupling of 90.8 MHz) corresponds to a p orbital spin density of 2.42% (2.2/90.8 × 100). In this limit no structural information could be obtained.

(36) Fortman, J. J.; Hayes, R. G. *J. Chem. Phys.* **1965**, *43*, 15.

(37) Williams, J.; Chasteen, N. D.; Moreton, K. *Biochem. J.* **1982**, *201*, 527–532.

(38) Chasteen, N. D.; Williams, J. *Biochem. J.* **1981**, *193*, 717–727.

(39) (a) Baldwin, D. *Biochim. Biophys. Acta* **1980**, *623*, 183–188. (b) Baldwin, D. A.; de Sousa, D. M. R. *Biochem. Biophys. Res. Commun.* **1981**, *99*, 1101–1107.

(40) Nishida, Y.; Oshio, S.; Kida, S. *Inorg. Chim. Acta* **1977**, *23*, 59.

(41) Anderson, B. F.; Baker, H. M.; Dodson, E. J.; Norris, G. E.; Rumball, S. V.; Waters, J. M.; Baker, E. N. *Proc. Natl. Acad. Sci. U.S.A.* **1987**, *84*, 1769.

(42) Anderson, B. F.; Baker, H. M.; Haridas, M.; Norris, G. E.; Rumball, S. V.; Smith, C. A.; Baker, E. N. *Abstracts*; XXVII International Conference on Coordination Chemistry; Brisbane, Australia, 1989; S20.

(43) McConnell, H. M.; Strathdee, J. *Mol. Phys.* **1959**, *2*, 127–138.

(44) Atherton, N. M. *Electron Spin Resonance*; Wiley: New York, 1973; pp 130–131.

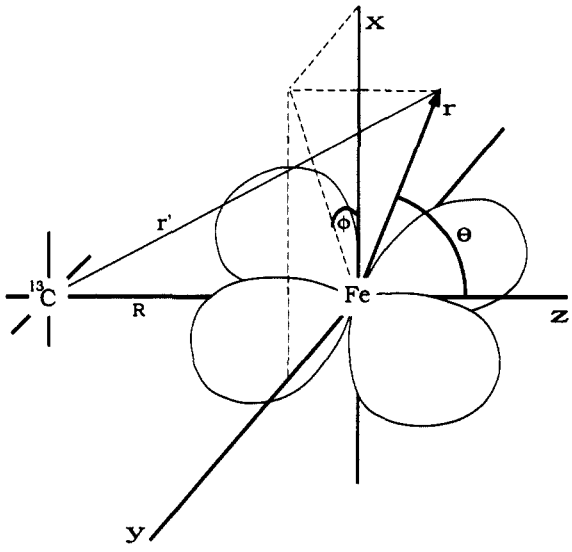

Figure 6. Coordinate system and variables used in calculating the electron–nuclear dipole interaction due to an unpaired electron in the metal-based d orbital as described in the Appendix.

Figure 6 shows the coordinate system used in calculating the coupling tensor. The tensor elements

$$t^0_{xx} = \int \Psi(r,\theta,\phi)\left(\frac{3x^2 - r'^2}{r'^5}\right)\Psi(r,\theta,\phi)\,d\tau$$

$$t^0_{yy} = \int \Psi(r,\theta,\phi)\left(\frac{3y^2 - r'^2}{r'^5}\right)\Psi(r,\theta,\phi)\,d\tau$$

$$t^0_{zz} = \int \Psi(r,\theta,\phi)\left(\frac{3z^2 - r'^2}{r'^5}\right)\Psi(r,\theta,\phi)\,d\tau$$

are calculated by use of the Slater $3d_{yz}$ orbital:

$$\Psi(r,\theta,\phi) = \frac{1}{81}\left(\frac{2K^3}{\pi}\right)^{1/2}\rho^2 \exp(-\rho/3)\sin\theta\cos\theta\sin\phi$$

where $K = z/a_0$ and $\rho = Kr$ (z is the effective nuclear charge; a_0 is the Bohr radius).

The operators are expressed in terms of the polar coordinates r, θ, ϕ

$$x = r\sin\theta\cos\phi \qquad y = r\sin\theta\sin\phi \qquad z = r\cos\theta$$
$$r'^2 = R^2 + r^2 + 2Rr\cos\theta$$

When r is written in terms of ρ and a is defined as $a = KR/2$, then the elements to be calculated are of the form

$$t^0_{xx} = \frac{2K^3}{(81)^2\pi}\int\int\int \rho^6 e^{-2\rho/3}\sin^3\theta\cos^2\theta\sin^2\phi \times \left[\frac{3\rho^2\sin^2\theta\cos^2\phi - 4a^2 - \rho^2 - 4a\rho\cos\theta}{(4a^2 + \rho^2 + 4a\rho\cos\theta)^{5/2}}\right] d\theta\,d\phi\,d\rho$$

$$t^0_{yy} = \frac{2K^3}{(81)^2\pi}\int\int\int \rho^6 e^{-2\rho/3}\sin^3\theta\cos^2\theta\sin^2\phi \times \left[\frac{3\rho^2\sin^2\theta\sin^2\phi - 4a^2 - \rho^2 - 4a\rho\cos\theta}{(4a^2 + \rho^2 + 4a\rho\cos\theta)^{5/2}}\right] d\theta\,d\phi\,d\rho$$

$$t^0_{zz} = \frac{2K^3}{(81)^2\pi}\int\int\int \rho^6 e^{-2\rho/3}\sin^3\theta\cos^2\theta\sin^2\phi \times \left[\frac{3\rho^2\cos^4\theta - 4a^2 - \rho^2 - 4a\rho\cos\theta}{(4a^2 + \rho^2 + 4a\rho\cos\theta)^{5/2}}\right] d\theta\,d\phi\,d\rho$$

where the limits of integration are $0 \le \theta \le \pi$, $0 \le \phi \le 2\pi$, and $0 \le \rho \le \infty$. The integration over ϕ is straightforward. The integrals over θ take on two values, one for $\rho < 2a$ and the other for $\rho > 2a$. The results for these integrals are

$$\int \sin^5\theta\cos^2\theta[4a^2 + \rho^2 + 4a\rho\cos\theta]^{-5/2}\,d\theta = \frac{1}{210a^5} + \frac{\rho^2}{252a^7};\ \frac{16}{105\rho^5} + \frac{128a^2}{63\rho^7}$$

$$\int \sin^3\theta\cos^2\theta[4a^2 + \rho^2 + 4a\rho\cos\theta]^{-5/2}\,d\theta = \frac{a^2 + \rho^2}{30a^5(4a^2 - \rho^2)};\ \frac{4\rho^2 + 64a^2}{15\rho^2(\rho^2 - 4a^2)}$$

$$\int \sin^3\theta\cos^3\theta[4a^2 + \rho^2 + 4a\rho\cos\theta]^{-5/2}\,d\theta = \frac{-3a^2\rho - \rho^3}{(21)(4)a^6(4a^2 - \rho^2)};\ \frac{-128a^3 - 24a\rho^2}{(21)\rho^6(\rho^2 - 4a^2)}$$

The integrals for calculating tensor elements for the other d orbitals with a point nucleus in other orientations are given in ref 45.

A final integration over ρ results in the tensor elements as a function of R and a:

$$t^0_{xx} = \frac{1}{R^3}\left[\left(\frac{-2048}{76545}a^6 - \frac{4096}{25515}a^5 - \frac{8288}{59049}a^4 - \frac{2176}{405}a^3 - \frac{232}{9}a^2 - \frac{316}{3}a - 111 - \frac{990}{a} - \frac{4185}{2a^2} - \frac{6075}{2a^3} - \frac{18225}{8a^4}\right)\exp(-4a/3) + \frac{135}{2a^2} + \frac{18225}{8a^4} - 1\right] \quad (A1)$$

$$t^0_{yy} = \frac{1}{R^3}\left[\left(\frac{-128}{729}a^5 - \frac{8224}{1701}a^4 - \frac{754}{81}a^3 - \frac{152}{3}a^2 - \frac{700}{3}a - 887 - \frac{2682}{a} - \frac{12123}{2a^2} - \frac{3^65^2}{2a^3} - \frac{3^75^2}{8a^4}\right)\exp(-4a/3) - \frac{(3)^3}{2a^2} + \frac{3^7(25)}{8a^4} - 1\right] \quad (A2)$$

Using the fact that $t_{zz} = -t_{xx} - t_{yy}$ gives

$$t^0_{zz} = \frac{1}{R^3}\left[\left(\frac{2048}{76545}a^6 + \frac{8576}{25515}a^5 + \frac{2056448}{3^{10}7}a^4 + \frac{5946}{(81)5}a^3 + \frac{688}{9}a^2 + \frac{1016}{3}a + 1246 + \frac{3672}{a} + \frac{8154}{a^2} + \frac{12150}{a^3} + \frac{18225}{2a^4}\right)\exp(-4a/3) - \frac{-54}{a^2} - \frac{18225}{2a^4} + 2\right] \quad (A3)$$

Note that, as would be expected, these tensor elements reduce to the case of a point dipole–dipole interaction when a is large, corresponding to a large distance between the electron and nucleus.

For the case of the d_{xy} orbital with nucleus along x

$$t'_{xx} = t^0_{zz} \qquad t'_{yy} = t^0_{yy} \qquad t'_{zz} = t^0_{xx}$$

where the 0 superscript represents the case calculated above and ′ represents the d_{xy}–x-axis problem.

The variable a is dependent on the effective nuclear charge, Z, and the distance, R. The Clementi rules[46] were used to obtain an approximate value for Z of 11.33. For large Z (as is the case for iron), the tensor elements calculated are relatively insensitive to small changes in Z. Changes in the value of Z by ±0.3 only change the dipolar elements by a maximum of ±0.02 MHz. Using R = 2.09 Å, which best matched the ^{13}C ENDOR data, and multiplying by $gg_n\beta_n\beta_e$ gives the dipolar terms

$$A_{d,xx} = 4.73\ \text{MHz} \qquad A_{d,yy} = -2.32\ \text{MHz}$$
$$A_{d,zz} = -1.78\ \text{MHz}$$

(45) Snetsinger, P. A. Ph.D. Thesis, University of New Hampshire, 1990.
(46) Clementi, E.; Raimondi, D. L. *J. Chem. Phys.* **1963**, *38*, 2686–2689.